From the Multiple-Well Master Equation to Phenomenological Rate Coefficients: Reactions on a C_3H_4 Potential Energy Surface

James A. Miller* and Stephen J. Klippenstein*

Combustion Research Facility, Sandia National Laboratories, Livermore, California 94551-0969

Received: September 19, 2002; In Final Form: February 4, 2003

Using various forms of electronic-structure theory to characterize the important features of the potential energy surface, RRKM theory to calculate microcanonical rate coeffients, and several formulations of the master equation to predict phenomenological rate coefficients, we have studied a number of reactions that occur on the C_3H_4 potential. We discuss the results in some detail and compare them with experiment when possible. Generally, the agreement with experiment is excellent. "Multiple-well effects" are emphasized throughout the discussion. We cast our results in the form of modified Arrhenius functions for use in chemical kinetics modeling.

I. Introduction

Resonantly stabilized free radicals (RSFR's) are generally thought to play an important role in the formation of aromatic compounds, polycyclic aromatic compounds (PAH's), and soot[1−3] in the combustion of aliphatic hydrocarbon fuels. The simplest and most important RSFR from a combustion chemistry point of view is propargyl (C_3H_3). The importance of propargyl in combustion derives from its ability to react with itself and form cyclic species,

$$\begin{aligned} C_3H_3 + C_3H_3 &\rightarrow \text{benzene} \\ &\rightarrow \text{phenyl} + H \\ &\rightarrow \text{fulvene} \end{aligned} \qquad \text{(R1)}$$

These product species then constitute the building blocks for the formation of PAH's and (ultimately) soot. Modeling such processes successfully requires not only knowledge of the rate coefficient and product distribution of reaction R1, but also knowledge of the rate coefficients for reactions that form propargyl and those that destroy it in competition with reaction R1.

In rich flames (where PAH compounds are found), C_3H_3 is normally formed either by the reaction of singlet methylene with acetylene,[3]

$$^1CH_2 + C_2H_2 \rightarrow C_3H_3 + H, \qquad \text{(R2)}$$

or by abstraction of a hydrogen atom from allene (C_3H_4a) or propyne (C_3H_4p). It can be destroyed in a number of ways, most notably by reaction with molecular oxygen,

$$C_3H_3 + O_2 \rightarrow CH_2CO + HCO, \qquad \text{(R3)}$$

although reaction R3 is extremely slow,[4] or by reaction with H or OH. In previous work, we have discussed reaction R1 in some detail in terms of the BAC-MP4 potential of Miller and Melius[3] and Melius et al.;[5] an article based on an improved potential is being prepared.[2] We have also discussed reaction R3 at some length,[4] and Blitz et al.[6] and Frankcombe and Smith[7] have treated reaction R2 theoretically using a master-equation (ME) approach. Harding and Klippenstein[8] have studied the barrierless addition of a hydrogen atom to propargyl using sophisticated electronic-structure methods and variational transition-state theory. In the present article, we supplement their work with new QCISD(T) electronic-structure calculations of the properties of several stationary points on the C_3H_4 potential; we then use this information to calculate a number of rate coefficients occurring on the potential using a combination of RRKM theory and various master-equation methods that we have developed.[4,9−15]

The reaction of H with propargyl, and the isomerization and dissociation reactions that accompany it, is a classic (yet simple) example of a reaction occurring over multiple, interconnected potential wells. Such reactions are ubiquitous in the chemistry of hydrocarbon growth in rich flames. Consequently, the present analysis allows us not only to provide important information for flame modeling, but also to exercise the tools mentioned in the preceding paragraph on a relatively simple problem, in preparation for more complex ones.

II. Theoretical Methodology

Harding and Klippenstein[8] have discussed at some length the potential energy surface (PES) for the addition of a hydrogen atom to both the CH_2 and CH ends of propargyl, as well as methods for obtaining microcanonical (RRKM) rate coefficients from the PES by variational transition-state theory. We use their methods and results in this work. Moreover, we have previously discussed our own methods for obtaining microcanonical isomerization rate coefficients, calculating densities and sums of states, and handling hindered rotations.[9,16] We shall not repeat that discussion here. However, we do discuss below our calculations of the important stationary points on the C_3H_4 potential and review our methodology for obtaining phenomenological rate coefficients from solutions to various forms of the master equation (ME), the most important of which is the time-dependent, multiple-well form. Tunneling is included in our rate-coefficient calculations one-dimensionally by assuming that the reaction path can be described by an Eckart function.

Quantum Chemistry. The geometric structures and vibrational frequencies for all stationary points considered here were obtained via density functional theory employing the Becke-3 Lee−Yang−Parr (B3LYP) functional[17] and the 6-311++G(d,p)

10.1021/jp0221082 CCC: $25.00
Published on Web 03/21/2003

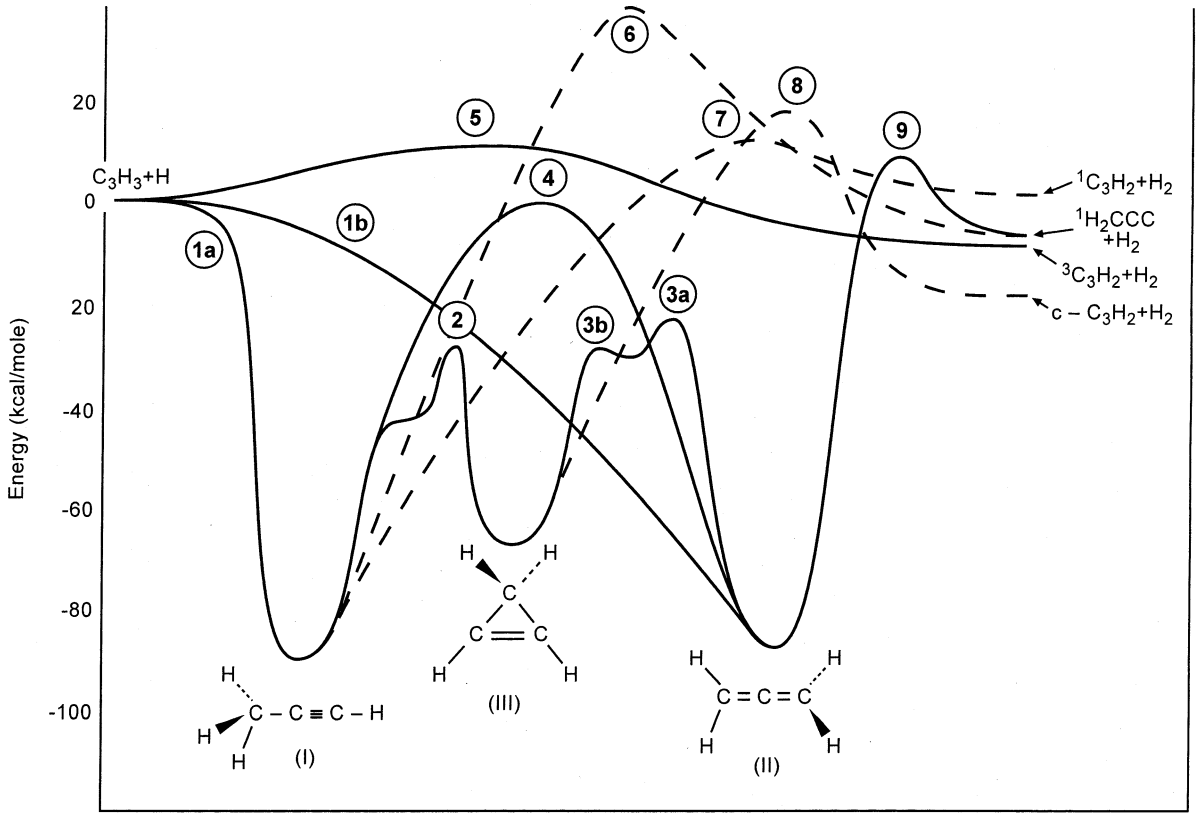

Figure 1. Schematic diagram of the C_3H_4 potential energy surface.

basis set.[18] Unrestricted wave functions were employed in these B3LYP optimizations and vibrational analyses. The connections of each saddlepoint to its local minima were generally estimated via visualization of the corresponding imaginary vibrational mode. For a few uncertain cases, intrinsic reaction coordinate calculations were also performed.

Higher-level energies were obtained via two separate methods. Both methods employ a combination of quadratic configuration-interaction calculations with perturbative inclusion of the triplet contribution, QCISD(T),[19] and second-order Møller−Plesset perturbation theory (MP2).[18] Spin-restricted wave functions were employed for all of the QCISD(T) and MP2 evaluations, except for those involving triplet states.

For the first method, the 6-311G(d,p) basis set is employed for the QCISD(T) calculations, and the 6-311++G(3df,2pd) basis set is employed for the MP2 calculations. Also, the core electrons are treated as active in the MP2 evaluations for the latter basis set. Approximate QCISD(T,full)/6-311++G(3df,-2pd) estimates, E_{HL1}, are then obtained as

$$E_{HL1} = E[\text{QCISD(T)/6-311G(d,p)}] + E[\text{MP2(full)/6-311++G(3df,2pd)}] - E[\text{MP2/6-311G(d,p)}] \quad (1)$$

For the second method, we estimate the infinite basis set limit via the extrapolation of results obtained for sequences of the correlation-consistent polarized-valence basis sets. The extrapolation is obtained from the expression,[20]

$$E(\infty) = E(l_{max}) - B/(l_{max} + 1)^4, \quad (2)$$

where l_{max} is the maximum angular momentum in the basis set. The QCISD(T) extrapolation is obtained on the basis of calculations with Dunning's correlation-consistent polarized-valence double-ζ (cc-pvdz) and triple-ζ (cc-pvtz) basis sets[21] with $l_{max} = 2$ and 3, respectively. An MP2 calculation with the correlation-consistent, polarized-valence, quadruple-ζ basis (cc-pvqz) ($l_{max} = 4$) allows for two separate MP2 extrapolations: one from the cc-pvdz, cc-pvtz pair and one from the cc-pvtz, cc-pvqz pair. The final higher-level estimate, E_{HL2}, is obtained as the sum of the QCISD(T) extrapolation and the difference between the two MP2 extrapolations. This combination of extrapolations can be expressed as

$$E_{HL2} = E[\text{QCISD(T)/cc-pvtz}] + \{E[\text{QCISD(T)/cc-pvtz}] - E[\text{QCISD(T)/cc-pvdz}]\} \times 0.462\,86 + E[\text{MP2/cc-pvqz}] + \{E[\text{MP2/cc-pvqz}] - E[\text{MP2/cc-pvtz}]\} \times 0.693\,77 - E[\text{MP2/cc-pvtz}] - \{E[\text{MP2/cc-pvtz}] - E[\text{MP2/cc-pvdz}]\} \times 0.462\,86 \quad (3)$$

Zero-point energy changes are evaluated at the B3LYP/6-311++G(d,p) level and are incorporated into the final energies reported below. The Gaussian 98 quantum chemistry software was employed in all of the quantum chemistry calculations described here.[22]

Master-Equation Methods. Figure 1 is a schematic diagram of the PES on which our analysis is based. It is useful to refer to it during the discussion that follows, although we defer discussing the electronic-structure calculations that produced it until the next section. The first point to notice is that there are four sets of bimolecular products, i.e., $C_3H_2 + H_2$ pairs. The $C_3H_3 + H$ configuration is viewed as a set of "bimolecular reactants". Only the reaction

$$C_3H_3 + H \rightarrow {}^3C_3H_2\ (\text{propargylene}) + H_2,$$

which is a direct abstraction, takes place on the triplet surface.

We calculate its rate coefficient independently by conventional transition-state theory. Other reactions of interest take place on the ground-state singlet surface, and their rate coefficients require solutions to the master equation.

Our master-equation formulation[9,10,15] envisions an environment where the $C_3H_3 + H$ rate coefficients can be measured under pseudo-first-order conditions, i.e.

$$n_d \gg n_m \gg n_R \tag{4}$$

where n_d is the number density of the diluent, n_m is the number density of the "excess" reactant (either C_3H_3 or H), and n_R is the number density of the deficient reactant. Under such conditions, the master equation, which is one-dimensional in the total internal energy E, is also linear and can be cast in the form[2,9,10,15]

$$\frac{d|w\rangle}{dt} = \mathbf{G}|w\rangle, \tag{5}$$

where $|w\rangle$ is a vector containing the populations of all of the relevant states and **G**, the transition matrix of the master equation, is real and symmetric. The solution to eq 5 can be written as

$$|w(t)\rangle = \hat{T}|w(0)\rangle, \tag{6}$$

where $|w(0)\rangle$ contains the initial condition and $\hat{T}$ is the time evolution operator,

$$\hat{T} = \sum_{j=0}^{N} e^{\lambda_j t}|g_j\rangle\langle g_j|. \tag{7}$$

The vectors $|g_j\rangle$ and the scalars λ_j are the eigenvectors and eigenvalues of **G**, i.e., $\mathbf{G}|g_j\rangle = \lambda_j|g_j\rangle$, $j = 0, ..., N$.

Although $N + 1$ is typically a very large number, only the "normal modes of relaxation" corresponding algebraically to the largest eigenvalues of **G** (the least negative ones) normally describe chemical change.[2,15,23−26] The remainder describe the relaxation of the internal degrees of the molecules in question. These latter modes typically relax much faster than the chemical ones, and it is only under such conditions that we can expect a phenomenological description of the chemistry to apply.[2,15,23−26] If there are S "species", or chemical configurations, there are

$$N_{chem} = S - 1 \tag{8}$$

chemically (or kinetically) significant eigenpairs of **G** (CSE's) in addition to $\lambda_0 = 0$ and $|g_0\rangle$, which describe a state of complete thermal and chemical equilibrium. Of course, all these eigenvalues are negative. We define λ_1 to be the largest (least negative) of the eigenvectors, λ_2 to be the second largest, and so on; $|g_1\rangle$, $|g_2\rangle$, ... are the corresponding eigenvectors. At the same time, for a problem with S distinct chemical configurations, there are N_k forward rate coefficients,[2] where

$$N_k = \frac{S(S-1)}{2}, \tag{9}$$

and an equal number of reverse rate coefficients or equilibrium constants. In the problem at hand (Figure 1), $S = 5$ because we have lumped all three of the $C_3H_2 + H_2$ "bimolecular products" formed on the singlet surface into one "infinite sink", and thus $N_{chem} = 4$. We discuss below how to deal with the infinite sinks as long as one is not interested in the rate coefficient from one sink to another. Because of this approximation, $N_k = 18$, rather than the 21 indicated by eq 9 with $S = 7$ (three sets of bimolecular products)—the three reactions that involve one set of bimolecular products reacting to form another are missing!

In a previous article,[15] we derived two methods of obtaining the rate coefficients from the CSE's. Both methods rely on representing the time evolution of the populations as

$$X_i(t) = \sum_{j=0}^{N_{chem}} a_{ij} e^{\lambda_j t} \quad (i = I, ..., M, R, p_1, p_2, p_3), \tag{10}$$

where M = III is the number of wells and $X_i(t)$ is the fraction of the initial reactant concentration (either one of the wells or the deficient reactant R of the $C_3H_3 + H$ pair) that is present in configuration i at time t. The p_α's ($\alpha = 1, ..., 3$) represent the different sets of bimolecular products:

$$p_1 = {}^1H_2CCC \text{ (singlet propadienylidene)} + H_2$$

$$p_2 = {}^1C_3H_2 \text{ (singlet propargylene)} + H_2$$

$$p_3 = \text{c-}C_3H_2 \text{ (singlet cyclopropenylidene)} + H_2$$

The coefficient $a_{i0} = X_i(\infty)$ is the "equilibrium" population of the ith configuration, and

$$a_{ij} = -\Delta X_{ij} \quad (j \neq 0), \tag{11}$$

where ΔX_{ij} is the change in population of the ith configuration that accompanies the time evolution of the jth eigenpair (jth term of eq 10) from $t = 0$ to $t = \infty$. The ΔX_{ij}'s and the λ_j's are the fundamental quantities needed to calculate the phenomenological rate coefficients. In principle, the ΔX_{ij}'s come from the eigenvectors of **G**. However, the infinite-sink approximation introduces some complications. Because of this approximation, λ_0 and $|g_0\rangle$ are absent from the spectrum of **G**, and $X_i(\infty) = 0$ for $i \neq p_\alpha$ ($\alpha = 1, ..., 3$) We describe below how to calculate $X_{p_\alpha}(\infty)$ and ΔX_{p_α} for multiple sinks, but first we review the rate-coefficient formulas.

In the article mentioned above, we adopted two different approaches to the problem of determining the phenomenological rate coefficients. The first utilizes different initial conditions and takes the limit of $dX_i(t)/dt$, from differentiating eq 10, as $t \rightarrow 0$ to derive expressions for the rate coefficients. The second method involves a single (but arbitrary) initial condition and exploits the time evolution of the system, through eq 10, from that initial condition. The rate-coefficient expressions are as follows:

method 1

$$\begin{aligned} k_{Ti} &= \sum_{j=1}^{N_{chem}} \lambda_j \Delta X_{ij}^{(i)} \\ k_{il} &= -\sum_{j=1}^{N_{chem}} \lambda_j \Delta X_{lj}^{(i)} \end{aligned} \tag{12}$$

method 2

$$\begin{aligned} k_{Ti} &= -\sum_{j=0}^{N_{chem}} \lambda_j a_{ij} b_{ji} \\ k_{il} &= \sum_{j=0}^{N_{chem}} \lambda_j a_{lj} b_{ji} \end{aligned} \tag{13}$$

The superscript on $\Delta X_{ij}^{(i)}$ in eq 12 indicates that the "reactant"

must be species i. If the a_{ij} are considered to be the elements of a matrix A, the b_{ij} are the elements of its inverse, $B = A^{-1}$. The rate coefficients k_{Ti} and k_{il} are the total rate coefficient for removal of species i and the $i \rightarrow l$ rate coefficient, respectively. If the process in question is actually bimolecular, these expressions give the pseudo-first-order rate coefficients and must be divided by n_m to get the true bimolecular rate coefficients. In most cases we use eqs 12 to calculate rate coefficients, because they are simpler computationally. Under the vast majority of conditions, the two methods yield the same values for the rate coefficients.

It remains to calculate ΔX_{lj} when l is one of the p_α's. From the solution to the master equation, we can determine $x_i(E,t)$, where $x_i(E,t)\,dE$ is the fraction of the initial reactant concentration present in well i with energy between E and $E + dE$ at time t,

$$x_i(E,t) = \sum_{j=1}^{N_{chem}} c_{ij}(E)\, e^{\lambda_j t}. \tag{14}$$

The coefficient $c_{ij}(E)$ comes from the jth eigenvector of **G**. Then, the rate of formation of p_α is

$$\frac{dX_{p_\alpha}}{dt} = \sum_{i=1}^{M} \int_{E_{0_i}}^{\infty} x_i(E,t)\, k_{ip_\alpha}(E)\, dE, \tag{15}$$

where $k_{ip_\alpha}(E)$ is the microcanonical rate coefficient for dissociation of i to p_α. Inserting eq 14 into eq 15 and reversing the order of the summations and integration, one obtains

$$\frac{dX_{p_\alpha}}{dt} = \sum_{j=1}^{N_{chem}} e^{\lambda_j t} \sum_{i=1}^{M} \int_{E_{0_i}}^{\infty} c_{ij}(E)\, k_{ip_\alpha}(E) dE. \tag{16}$$

Integrating eq 16 term-by-term from zero to infinity (and remembering that λ_j is always negative), we get

$$\Delta X_{p_\alpha j} = -\frac{1}{\lambda_j} \sum_{i=1}^{M} \int_{E_{0_i}}^{\infty} k_{ip_\alpha}(E)\, c_{ij}(E)\, dE \tag{17}$$

and

$$X_{p_\alpha}(\infty) = \sum_{j=1}^{N_{chem}} \Delta X_{p_\alpha j} \tag{18}$$

Equations 17 and 18 can be used in eqs 12 and 13 to determine the phenomenological rate coefficients.

At low temperatures, it can be difficult numerically to obtain accurate eigenvalues and eigenvectors for **G**.[7,12] This problem can be overcome in either of two ways: (1) by doing the diagonalization in quadruple-precision arithmetic, rather than double precision[7] or (2) by integrating the ME directly in time[12] using an ODE solver, resorting to the "exponential-decay" approach[9−12] to determine rate coefficients and product distributions.

We have used both of these methods at various times in the present work. The latter approach is generally accurate at low temperatures, where the CSE's are well separated in magnitude and "interference effects" such as those described in ref 15 can be avoided.

The master equation described above is one-dimensional with E the independent variable. For two types of problems we can solve a two-dimensional (as well as one-dimensional) ME with E and J the independent variables, where J is the total angular-momentum quantum number: (1) The first is the zero-pressure (or collisionless) limit of a bimolecular reaction. This method is a generalization of that first derived by Miller et al.[14] and is described in the article by Hahn et al.[4] (2) The second is a one-well (but multiple-product), irreversible dissociation or isomerization. This method is described in detail by Miller, Klippenstein, and Raffy.[13] We use both of these methods in the analysis presented below.

In all master-equation calculations, we use a single exponential-down model for $P(E,E')$, the energy transfer function. Various bath gases are considered, and the values of $\langle \Delta E_d \rangle$ used in the calculations are discussed as the situation arises. However, for argon and krypton we found it convenient to use the expression

$$\langle \Delta E_d \rangle = 133 \left(\frac{T}{300\ K} \right)^{0.85} cm^{-1} \tag{19}$$

in all our calculations, independent of E. This expression is loosely based on our experience with CH_4 dissociation[13] and gives good results in the present work. Examining the effects of changing $\langle \Delta E_d \rangle$, or more generally $P(E,E')$, is beyond the scope of the present work.

All of the rate-coefficient calculations reported here were done with VARIFLEX.[27]

III. Results and Discussion

Potential Energy Surface. The C_3H_4 potential energy surface has been the subject of a large number of prior theoretical analyses.[5,8,28−43] Taken together, these studies provide a reasonably complete description of the low-energy isomerization and decomposition pathways of the three primary isomers [propyne (I), allene (II), and cyclopropene (III)]. However, no single investigation has considered all aspects relevant to the thermal kinetics. In the interest of developing a consistent high-level model, we have undertaken a reanalysis of all of the stationary points relevant to the thermal isomerization/dissociation kinetics of the three primary isomers, employing the same high-level ab initio methodologies throughout. For completeness, we summarize these results here, noting that there is no conceptual change from conclusions obtained in these earlier studies.

The present results for the stationary-point energies, including zero-point corrections, are provided in Table 1. A schematic diagram of the potential energy surface obtained on the basis of the HL1 calculations is provided in Figure 1. Cyclopropylidene (cyclic-CH_2CCH_2) and the transition states that connect it with allene and cyclopropene (ts10 and ts11) have been omitted from this diagram, and from the kinetic analysis, because they should not play a significant role in the thermal kinetics.

Methylvinylidene (CH_3CHC) is predicted to be a local minimum at the B3LYP/6-311++G(d,p) level. However, limited attempts to locate the saddlepoint for formation of propyne from it were unsuccessful, apparently due to the smallness of the barrier. Indeed, it is unclear whether or not a saddle point even exists. The smallness of this barrier also makes this state kinetically irrelevant, and so it was not included in the kinetic analysis.

For the linear CH_2CHCH species, the spin contamination in the B3LYP calculations is extraordinarily large, and the corresponding higher-level energies are actually greater than those for the saddle point connecting it with cyclopropene. Spin-restricted B3LYP calculations yield a greatly different geometry. Interestingly, at the spin-restricted geometry, the higher-level energies are signifcantly below the corresponding saddle-point energy.

TABLE 1: Stationary-Point Energies for the C_3H_4 System Relative to $C_3H_3 + H$

species	E_{B3LYP}[a] (kcal/mol)	$E_{QCISD(T)}$[b] (kcal/mol)	E_{HL1}[c] (kcal/mol)	E_{HL2}[d] (kcal/mol)	$<S^2>$ (B3LYP)
wells					
CH_3CCH (I)	−85.6	−89.4	−89.8	−90.8	0
CH_2CCH_2 (II)	−87.6	−88.5	−89.1	−89.8	0
cyclic-CH_2CHCH (III)	−61.3	−65.7	−66.6	−67.1	0
CH_3CHC:	−39.5	−43.1	−42.6	−43.6	0
CH_2CHCH:	−31.4	−23.5	−24.5	−24.5	0.91
CH_2CHCH:[e]	−26.3	−28.3	−28.2	−29.2	0
cyclic-CH_2CCH_2	−21.0	−22.9	−23.3	−23.6	0.11
saddlepoints					
ts2 (I ↔ III)	−23.3	−28.5	−28.9	−29.7	0
ts3a (II ↔ CH_2CHCH)	−22.0	−22.2	−22.4	−23.4	0.02
ts3b (CH_2CHCH ↔ III)	−26.1	−28.1	−28.2	−29.1	0
ts4 (I ↔ II)	4.4	0.2	−0.7	−1.2	0
ts5 (R ↔ p_2)	4.3	10.3	10.8	10.1	2.04
ts6 (I ↔ p_3)	41.6	37.0	37.3	36.2	0
ts7 (I ↔ p_4)	9.1	11.6	11.7	10.3	0.16
ts8 (III ↔ p_1)	20.1	18.5	17.1	16.6	0
ts9 (II ↔ p_3)	2.8	3.9	3.9	2.9	0
ts10 (II ↔ cyclic-CH_2CCH_2)	−14.2	−16.6	−17.4	−17.7	0
ts11 (cyclic-CH_2CCH_2 ↔ III)	−5.5	−10.6	−11.6	−11.8	0
products					
cyclic-$CHCCH + H_2$ (p_3)	−14.8	−17.2	−17.9	−18.9	0
$^3CHCCH + H_2$ (p_4)	−11.0	−7.1	−6.3	−7.1	2.05
$CH_2CC + H_2$ (p_1)	−3.5	−4.9	−4.4	−5.1	0
$CHCCH + H_2$ (p_2)	4.3	6.1	6.2	5.2	0

[a] B3LYP/6-311++G(d,p) energies. [b] QCISD(T)/cc-pvtz energies. [c] HL1 energies according to eq 1. [d] HL2 energies according to eq 2. [e] Calculations at B3LYP/6-311++G(d,p) spin-restricted geometry.

TABLE 2: Heats of Formation

species	ΔH_f^0 (0 K) (kcal/mol) HL1	ΔH_f^0 (0 K) (kcal/mol) HL2	ΔH_f^0 (298 K) (kcal/mol) HL1	ΔH_f^0 (298 K) (kcal/mol) HL2
reactants				
C_3H_3	84.9	84.7	84.5	84.3
H	51.2	51.8	51.6	52.3
wells				
CH_3CCH (I)	46.3	45.7	44.8	44.2
CH_2CCH_2 (II)	46.9	46.8	45.3	45.2
cyclic-CH_2CHCH (III)	69.4	69.4	67.5	67.5
products				
cyclic-$CHCCH + H_2$ (p_3)	118.1	117.6	118.1	117.6
$^3CHCCH + H_2$ (p_4)	129.7	129.5	129.6	129.4
$CH_2CC + H_2$ (p_1)	131.6	131.4	132.3	132.1
$CHCCH + H_2$ (p_2)	142.2	141.7	143.8	143.3

The HL1 and HL2 results in Table 1 are remarkably similar, with only a single energy differing by more than 1.1 kcal/mol, and with even that one differing by only 1.4 kcal/mol. For all but the transition states connecting to H_2 products, the HL1 energies tend to be ~1 kcal/mol below the HL2 energies, suggesting that the primary difference between the two methods lies in their predictions for simple bond fission to $C_3H_3 + H$. It is also interesting to note that the QCISD(T)/cc-pvtz results tend to lie between the HL1 and HL2 results.

The kinetic analysis presented below employs the HL1 energies as a starting point, making only modest revisions as required to reproduce specific experimental results. Very similar kinetic results would be obtained for the HL2 energies, since the isomerization barriers relative to the minima are nearly identical. Furthermore, the difference of 1.0 kcal/mol for the dissociation threshold is only of minor significance at the high temperatures where dissociation is significant. For reference purposes, we have converted both the HL1 and HL2 energies for the stable species to heats of formation at 0 and 298 K using related calculations for CH_4 and H_2 to define the absolute scale (cf. Table 2). The thermal corrections for these heats of formation were obtained on the basis of rigid-rotor, harmonic-oscillator estimates. Importantly, the use of molecular (i.e., CH_4 and H_2), rather than atomic, references ameliorates a number of errors, such as those due to anharmonic effects, spin−orbit effects, etc.

In Table 3, the present HL1 results are contrasted with a variety of earlier results. As might be expected, the CCSD(T)/6-311+G(3df,2pd) results of Mebel et al.[42] and the G2(B3LYP) results of Wang and co-workers[43] are quite similar to the present results. In contrast, the ICCI results of Walch[37] differ quite substantially. In this regard, it is worth noting that the Davidson correction ($+Q$), which provides some measure of the expected accuracy, is typically about 5 kcal/mol for these calculations.

Chemical Kinetics. As noted above, the stationary-point energies shown in Figure 1 are largely drawn from the HL1 calculations (eq 1). The only exception is that E_{03a} and E_{03b} (the ground-state energies of ts3a and ts3b, respectively) were each reduced by 490 cm^{-1}, and E_{02} was reduced by 20 cm^{-1} to optimize the agreement of the theory with the experiments of Bailey and Walsh,[44] discussed below. Such changes are well within the accuracy of the quantum-chemical methods employed and, for that matter, within the accuracy of virtually all methods in common use. All of the calculations then were done with the same PES parameters. We should note also that the shallow well between ts3a and ts3b, corresponding to the linear CH_2-$CHCH$ configuration, is assumed to be collisionless, and the sum of states $N_3^{\ddagger}$ is approximated by the formula

$$N_3^{\ddagger} = N_{3a}^{\ddagger} N_{3b}^{\ddagger} / (N_{3a}^{\ddagger} + N_{3b}^{\ddagger}) \qquad (20)$$

In practice, it is only ts3a that matters, because it is the higher of the two saddlepoints. Of course, this is reflected in eq 20.

It is instructive to examine the eigenvalue spectrum of **G** in the present case to see how the CSE's separate in magnitude from what is essentially a continuum of energy-transfer eigenvalues. (Typically, the separation between adjacent eigenvalues in the continuum is not more than a few percent.) This is shown in Figure 2, which is a plot of the eigenvalue spectrum as a function of temperature for $p = 1$ atm. The physical significance

TABLE 3: Stationary-Point Energies from Various Different Studies for the C_3H_4 System Relative to $C_3H_3 + H$[a]

species	HL1[b]	CCSD(T)[c]	G2[d]	ICCI[e] (no Q)	ICCI[f] + *Q*
wells					
CH_3CCH (I)	−89.8	−88.7	−89.8	−84.6	−87.9
CH_2CCH_2 (II)	−89.1	−87.8	−88.7	−81.9	−86.2
cyclic-CH_2CHCH (III)	−66.6	−65.9	−65.9	−57.6	−62.1
CH_3CHC:	−42.6			−35.5	−40.9
CH_2CHCH:	−28.2			−19.1	−24.7
cyclic-CH_2CCH_2	−23.3			−9.4	−17.4
saddlepoints					
ts2 (I ↔ III)	−28.9		−29.6	−18.8	−27.1
ts3a (II ↔ CH_2CHCH)	−22.4		−24.4	−12.8	−19.5
ts3b (CH_2CHCH ↔ III)	−28.2		−28.3	−11.6	−19.0
ts4 (I ↔ II)	−0.7				
ts5 (R ↔ p_2)	10.8				
ts6 (I ↔ p_3)	37.3	38.4			
ts7 (I ↔ p_4)	11.7	11.9			
ts8 (III ↔ p_1)	17.1				
ts9 (II ↔ p_3)	3.9	4.6			
ts10 (II ↔ cyclic-CH_2CCH_2)	−17.4			−6.5	−13.2
ts11 (cyclic-CH_2CCH_2 ↔ III)	−11.6			0.8	−6.0
products					
cyclic-$CHCCH + H_2$ (p_3)	−17.9	−18.3			
$^3CHCCH + H_2$ (p_4)	−6.3	−7.0			
$CH_2CC + H_2$ (p_1)	−4.4	−4.8			
$CHCCH + H_2$ (p_2)	6.2	5.6			

[a] All energies in kcal/mol. [b] Present HL1 energies. [c] CCSD(T)/6-311+G(3df,2p)//B3LYP/6-311G(d,p) energies from Mebel et al.[42] [d] G2(B3LYP) energies from Wang and co-workers.[43] This work does not provide a value for $C_3H_3 + H$ and so the value for propyne was taken as a reference and set to the HL1 value of −89.8 kcal/mol. [e] Internally contracted configuration interaction values without the Davidson correction for a valence triple-ζ basis (from Walch[37]). [f] Internally contracted configuration interaction values including the Davidson correction for a valence triple-ζ basis (from Walch[37]).

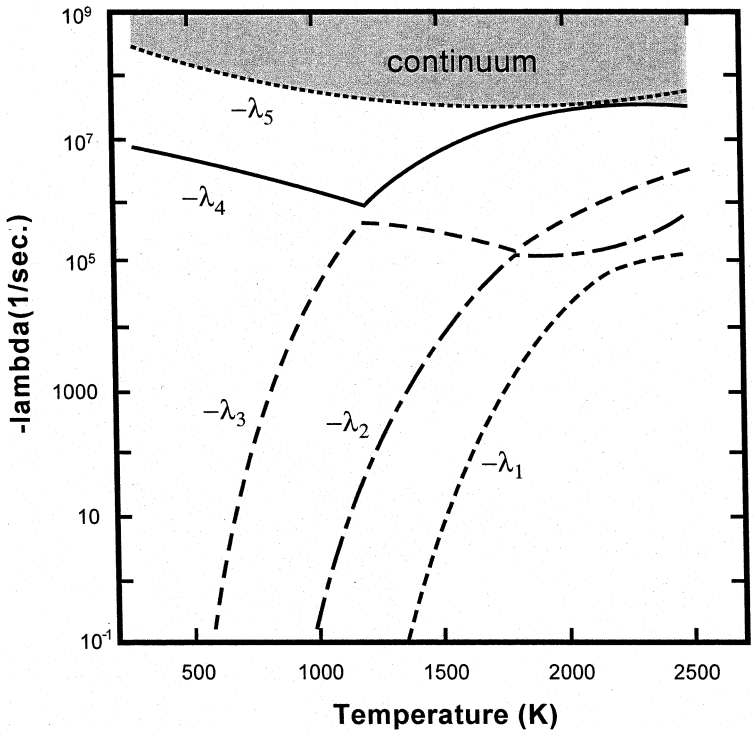

Figure 2. Eigenvalue spectrum of the **G** matrix as a function of temperature for a pressure of 1 atm.

of the eigenpairs can best be seen by considering an initial condition in which the entire population is present as $C_3H_3 + H$. In this case, at low temperature, λ_4 and $|g_4\rangle$ describe the equilibration of $C_3H_3 + H$ with propyne (C_3H_4p) (although other species may be formed at the same time), λ_3 and $|g_3\rangle$ describe the equilibration of these two species with cyclopropene (c-C_3H_4), and λ_2 and $|g_2\rangle$ bring about the equilibration of $C_3H_3 + H$, C_3H_4p, and c-C_3H_4 with allene (C_3H_4a). Finally, λ_1 and $|g_1\rangle$ describe the slow leak of this equilibrated "four-component" system to the $C_3H_2 + H_2$ pairs. As discussed previously, one can generally associate a transition state with an eigenvalue.[2,9−12] This association is quite pronounced at low *T* and persists, at least loosely, to high temperatures. In the present case, ts1 correlates with λ_4, ts2 with λ_3, ts3 with λ_2 , and principally it is ts7 and ts9 that correlate with λ_1. The other transition states play a relatively minor role in the kinetics. If this correlation is used to label the eigenvalue curves (it is *not* used in Figure 2), there are obvious crossings and/or avoided crossings[11] that occur

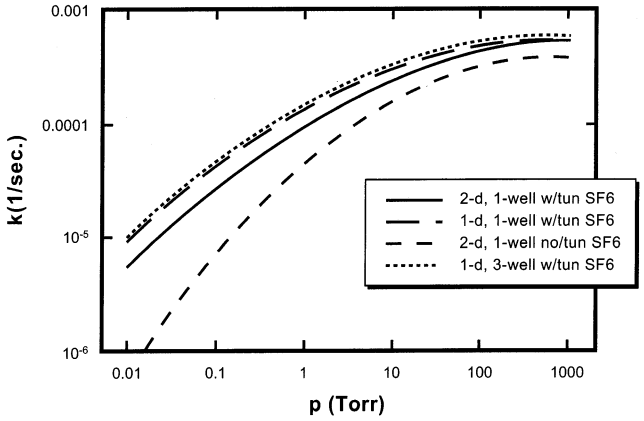

Figure 3. Falloff curves for c-$C_3H_4 \rightarrow C_3H_4p$ at $T = 495$ K using SF_6 as the collider. $\langle \Delta E_d \rangle$ was taken to be 700 cm^{-1} in all cases.

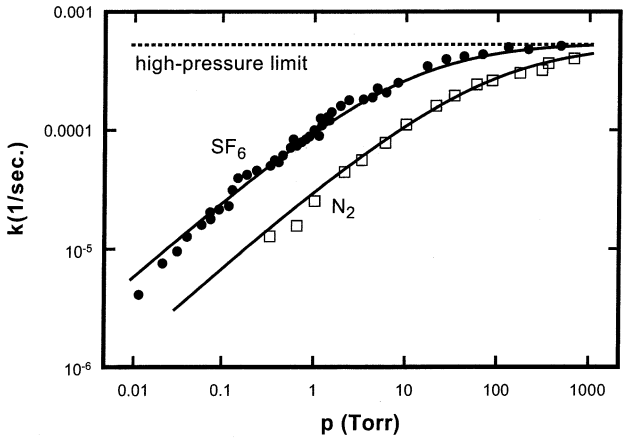

Figure 4. Comparison of the theory with the experiments of Bailey and Walsh[44] for the falloff of the c-$C_3H_4 \rightarrow C_3H_4p$ rate coefficient at 495 K. $\langle \Delta E_d \rangle$ for SF_6 was deduced to be 700 cm^{-1}; for N_2, it was determined to be 125 cm^{-1}.

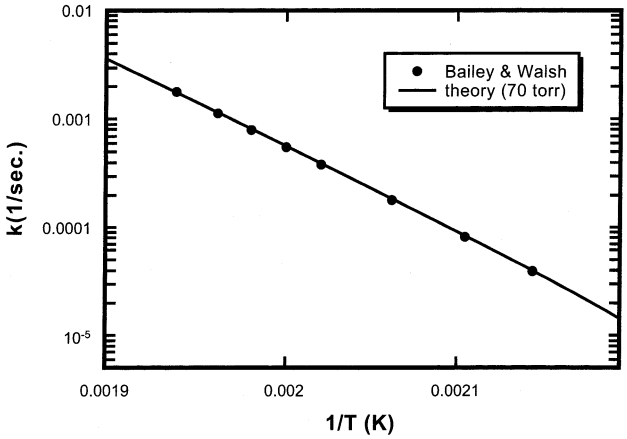

Figure 5. Comparison of the theory with the experiments of Bailey and Walsh[44] for the rate coefficient of c-$C_3H_4 \rightarrow C_3H_4p$ at $p = 70$ Torr. The filled circles are points along the Arrhenius expression given by Bailey and Walsh, not experimental points.

at higher temperatures. In particular, there is a crossing between the eigenvalue curves associated with ts1 and ts2 at $T \approx 1200$ K; ts2 correlates with λ_4 at high temperature.

The most important point to notice in Figure 2 is that the separation between the CSE's and the continuum, as well as between the CSE's themselves, becomes markedly reduced at high temperature. In the present case, λ_4 essentially *merges with the continuum* at $T \approx 2200$ K. This signals that c-C_3H_4 at this point has ceased to be a distinct chemical species in the kinetic sense discussed above. It equilibrates with C_3H_4p on a time scale that is roughly the same as the time scales associated with the relaxation of the internal energy. (Remember that ts2, which separates c-C_3H_4 from C_3H_4p, is associated with λ_4 at high T). In principle, this creates a problem for the validity of the rate-coefficient approximation, but in practice, one can assume c-C_3H_4 and C_3H_4p to be a single species (which is virtually all C_3H_4p). Then, in the analysis, we take $S = 4$ instead of 5, and N_{chem} becomes 3 instead of 4 in the equations of section II. This procedure results in good values for the thermal rate coefficients when taking $N_{chem} = 4$ is obviously incorrect (frequently, rate coefficients become negative for $T \geq 2200$ K with $N_{chem} = 4$).

At sufficiently high temperature, all of the CSE's eventually merge with the continuum (at least in the absence of the infinite sinks), and internal-energy relaxation and reaction become indistinguishable. It is worthwhile to note that the eigenvalues in the continuum (λ_5 and higher) have magnitudes that are linear in the pressure ($-\lambda_j \propto p$ for $j \geq 5$), whereas the CSE's are generally much weaker functions of pressure. This means that the CSE's merge into the continuum at higher temperatures as the pressure increases, and the rate coefficient approximation remains valid to higher temperatures for larger values of p.

Isomerization of Cyclopropene at Low Temperature. Bailey and Walsh[44] have studied the isomerization of cyclopropene to propyne and allene in the laboratory over a wide range of pressures in the temperature range 466 K < T < 516 K. Predicting their results theoretically depends critically on having accurate transition-state energies, E_{03} and E_{02}; it is on the basis of their experimental results that we made the adjustments to the transition-state energies mentioned above. To determine what ME methodology we should employ in comparisons with their experiments, consider Figure 3, which is a falloff plot at $T = 495$ K for cyclopropene isomerization to propyne with SF_6 as the bath gas; this is one of the experiments performed by Bailey and Walsh. Only theoretical results are shown on the plot. By comparing the one-dimensional/single-well result with that from the 1-d/3-well ME, we can conclude that multiple-well effects are not important at these temperatures and pressures. However, this is not necessarily the case at higher temperatures. The small difference between the predictions from these two methods shown in the figure is due to an automatic rebinning strategy employed in the state-counting algorithm used in VARIFLEX and is not physically significant. Discrepancies on the order of a few percent are common in comparisons of different methods for this reason. Other comparisons in Figure 3 clearly indicate that tunneling and angular-momentum conservation are important under these conditions. The same conclusion is drawn from looking at the product distributions. Consequently, the following comparisons are made with the 2-d/1-well formulation of the master equation with tunneling.

Figure 4 compares our predictions of the pressure dependence of the c-$C_3H_4 \rightarrow C_3H_4p$ rate coefficient at 495 K with the experimental results of Bailey and Walsh for both SF_6 and N_2 diluents. From these comparisons we deduce values for $\langle \Delta E_d \rangle$ of 125 cm^{-1} for N_2 and 700 cm^{-1} for SF_6. Davis et al.,[43] in considering the same data, deduced a value of $\langle \Delta E_d \rangle$ for N_2 of 260 cm^{-1}. This discrepancy is due predominantly to the neglect of tunneling in their analysis. Although one-dimensional tunneling calculations have their flaws, we believe that it is better to include tunneling in this fashion than to neglect it.

Figure 5 compares our prediction of the c-$C_3H_4 \rightarrow C_3H_4p$ rate coefficient with the data of Bailey and Walsh at $p = 70$ Torr in the temperature range 466 K < T < 516 K. The

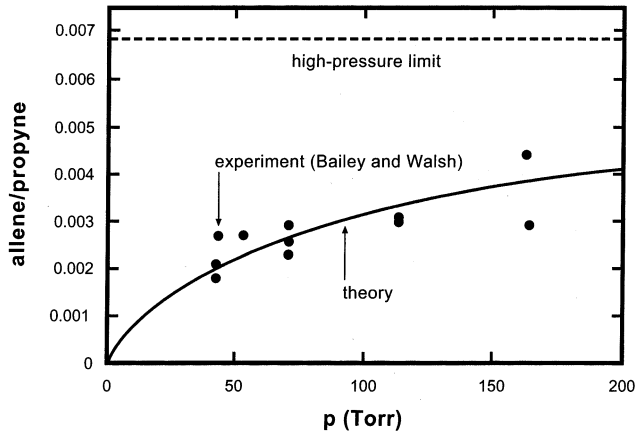

Figure 6. Comparison of the theory with the experimental results of Bailey and Walsh for the ratio of allene to propyne in the products of c-C_3H_4 isomerization at 495 K.

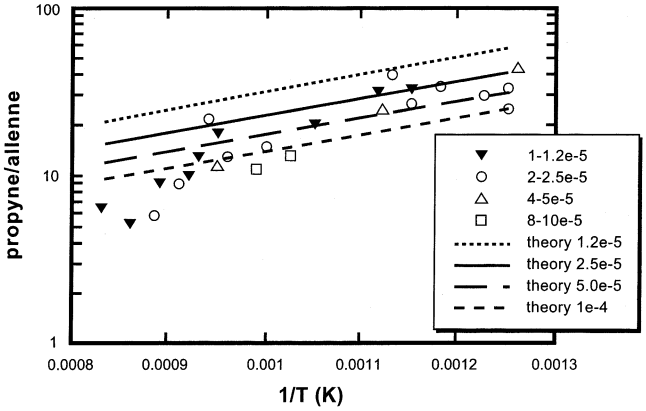

Figure 7. Comparison of the theory with the experiments of Karni et al.[32] for the propyne/allene ratio in the products of c-C_3H_4 isomerization.

agreement is almost perfect. The comparisons shown in Figures 4 and 5 give us considerable confidence in our theoretical model. However, the most severe test of the model is the product distribution in the cyclopropene isomerization.

In Figure 6, we compare our predictions for the allene/propyne ratio in the products of the c-C_3H_4 isomerization as a function of pressure at $T = 495$ K with the experimental data of Bailey and Walsh. The agreement between theory and experiment is again excellent. It is interesting that Bailey and Walsh, in interpreting their experiments, conclude that, if they threw away the highest point on the graph, their allene/propyne ratio would be independent of pressure. They believed that their experiments were very near the high-pressure limit and, thus, that this ratio should be constant. The present analysis indicates that, whereas the total rate coefficient (predominantly forming propyne) is close to the high-pressure limit under these conditions, the product distribution is far from it. At $p = 100$ Torr, Figure 6 shows that the allene/propyne ratio is less than half of its limiting high-pressure value.

Karni et al. [32] have also studied the product distribution in the isomerization of c-C_3H_4, although their experiments were performed at higher temperatures, 800 K < T < 1200 K, and higher pressures (predominantly in excess of 1 atm) than those of Bailey and Walsh. We compare our predictions for the C_3H_4p/C_3H_4a ratio with their experimental results in Figure 7. Both theory and experiment utilized argon as the bath gas. The theory shows a significant dependence of this product ratio on the number density of the diluent, a dependence that the scatter in the data appears to be too large to detect. Nevertheless, the

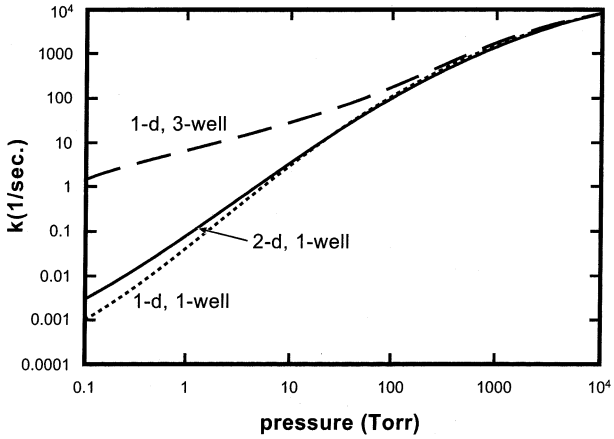

Figure 8. Theoretical falloff curves for c-C_3H_4 → C_3H_4a at $T = 1000$ K using various forms of the master equation.

agreement between theory and experiment is quite good. The theoretical results plotted in Figure 7 were obtained from the 2-d/1-well master equation. Calculations with the 1-d/3-well ME differ minimally from those plotted. Also, because of the pressures involved, the predictions of Figure 7 are relatively insensitive to realistic changes in $\langle \Delta E_d \rangle$.

Figure 8 shows an interesting phenomenon that we discovered in studying the product distribution in the isomerization of cyclopropene. The figure displays theoretical falloff curves at $T = 1000$ K for the minor channel c-C_3H_4 → a-C_3H_4 in the cyclopropene isomerization; various forms of the master equation, all of which include tunneling, were employed in generating the curves. Surprisingly, the 3-well curve deviates more and more from the 1-well results as the pressure is reduced. The 3-well result is roughly 3 orders of magnitude larger than the 1-well prediction at 0.1 Torr. This is a consequence of c-C_3H_4 complexes that isomerize to propyne and return almost immediately, ultimately isomerizing to allene instead, perhaps after suffering one or more activating collisions as cyclopropene or propyne. Remember that, in the 1-well model, the isomerizations are "irreversible", making the allene and propyne wells infinite sinks. It is probably significant that $E_{03a} - E_{0II}$ (E_{03a} and E_{0II} are the ground-state energies for ts3a and well II, respectively) is larger than $E_{02} - E_{0I}$ (even though the propyne well is deeper with respect to $C_3H_3 + H$), making the lifetimes in the allene well at energies of interest longer than those in the propyne well. There are no analogous multiple-well effects on the c-C_3H_4 → C_3H_4p isomerization rate coefficient; the effect described here is inconsequential as far as this latter reaction is concerned.

Figure 8 also shows that angular-momentum conservation is relatively unimportant at pressures that are likely to be of practical interest (perhaps $p \geq 10$ Torr), at least at high T. The same conclusion can be drawn from calculations of the c-C_3H_4 → C_3H_4p rate coefficient. Consequently, the 1-d/3-well ME is likely to give an accurate description of higher-temperature isomerization and dissociation processes. It is used in the remainder of the collisional ME calculations reported in this article.

Allene ⇄ Propyne Isomerization. An important advantage of the master-equation formalism is that it yields rate coefficients *unambiguously* for isomerization reactions that "skip a well". Except under special conditions, it is difficult to predict such rate coefficients accurately (in a systematic way) by more approximate, modified strong-collider methods. In the present case, even though any particular complex must pass through cyclopropene (and suffer any number of collisions there) to get from allene to propyne (or the reverse), the formalism described in section II and in ref 5 predicts that allene ⇄ propyne is a

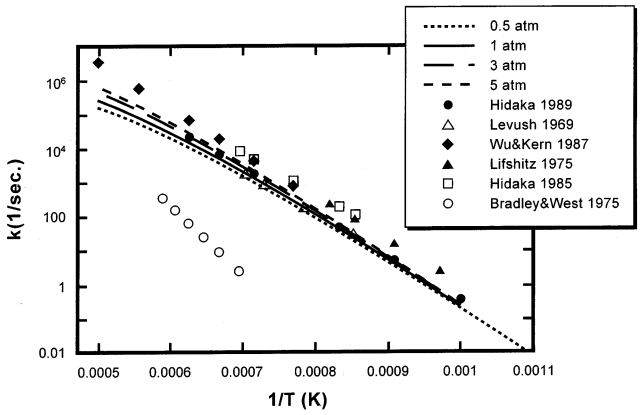

Figure 9. Comparison of theory with experiment for the $C_3H_4a \rightarrow C_3H_4p$ rate coefficient. The pressures used in the experiments were Hidaka et al. (1989),[46] 1.7−2.6 atm; Wu and Kern,[45] 0.2−0.5 atm; Hidaka et al. (1985),[49] 1.4−2.3 atm; Lifshitz et al.,[48] 1.2−6.0 atm; Levush et al.,[47] ∼1 atm; Bradley and West,[50] 3.95−5.26 atm. The symbols are points of the Arrhenius functions given by the authors, not experimental data points.

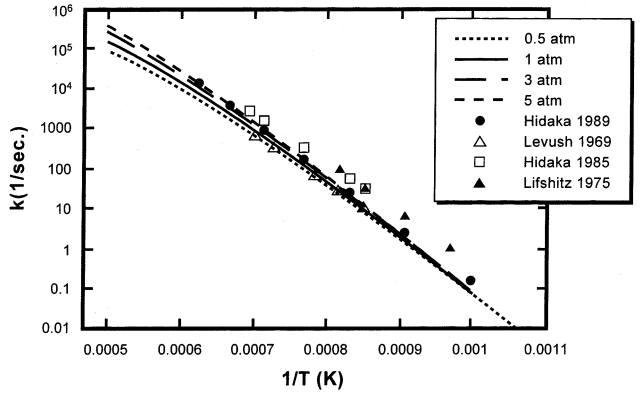

Figure 10. Comparison of the theory with experiment for the $C_3H_4p \rightarrow C_3H_4a$ rate coefficient. See Figure 9 for the pressures of the experiments. The symbols are points of the Arrhenius functions given by the experimentalists, not experimental data points.

perfectly good *elementary* reaction and gives its phenomenological rate coefficient quantitatively.

The allene ⇄ propyne isomerization has been studied extensively in the laboratory in both directions. In Figures 9 and 10, we compare our predictions for these rate coefficients with the experimental results available. In the calculations, we used argon as the bath gas, as did all of the experiments shown except those of Wu and Kern,[45] who diluted the reactant, allene, in neon. It is unlikely that the differences between theory and the Wu and Kern experiments shown in the figures can be attributed to different bath gases, because the theory shows that, at least near the lower end of the temperature range, both the forward and reverse rate coefficients are very near their high-pressure limits (i.e., there is very little pressure dependence). In general, the agreement between theory and experiment is quite good. We find particularly good agreement with the later experiments[46] from Hidaka's laboratory and with those of Levush et al.[47] Our rate coefficients are somewhat smaller than the experimental results of Wu and Kern,[45] Lifshitz et al.,[48] and the earlier work of Hidaka et al.[49] The experiments of Bradley and West[50] are inconsistent with both the theory and the other experiments.

Kiefer et al.[36] and Davis et al.[43] have also treated the allene ⇄ propyne isomerization theoretically using approximate, modified strong-collider methods. The latter obtained results

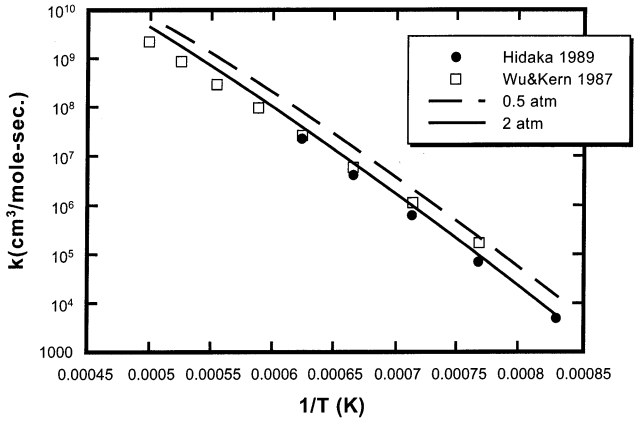

Figure 11. Comparison of the theory for the rate coefficient of $C_3H_4a + Ar \rightarrow C_3H_3 + H + Ar$ with the experiments of Hidaka et al.[46] and Wu and Kern.[45] The pressures of the experiments are given in Figure 9. The symbols are points of the Arrhenius functions given by the experimentalists, not experimental data points.

very similar to ours; the former predicted rate coefficients more in line with the experiments of Wu and Kern and Lifshitz et al. The three theoretical treatments (including the present one) all use somewhat different PES and energy-transfer parameters, as well as different variants of unimolecular rate theory (and different approximations in the modified strong-collider treatments). Consequently, comparisons among the theoretical treatments are probably not very meaningful.

Dissociation of Allene and Propyne. Because of the fast allene ⇄ propyne isomerization at high temperatures, where their dissociation rates are fast enough to be measured, distinguishing between the dissociations of the two isomers is quite difficult experimentally. Referring to Figure 2 (which is for $p = 1$ atm), for $T > 1800$ K, λ_3 and $|g_3\rangle$ describe the equilibration of allene with propyne and cyclopropene (which have themselves been equilibrated on the time scale $-1/\lambda_4$), and λ_2 and $|g_2\rangle$ describe (approximately) the dissociation of the three equilibrated isomers (c-C_3H_4 is negligible in this equilibrium, however) to $C_3H_3 + H$. At $T = 2000$ K, $-\lambda_3$ is greater than $-\lambda_2$ by more than a factor of 3, so that equilibration of all the isomers takes place faster than dissociation can occur. Consequently, most experiments are likely to be sensitive only to $-\lambda_2$, and not to the individual $C_3H_4p \rightarrow C_3H_3 + H$ and $C_3H_4a \rightarrow C_3H_3 + H$ dissociation rate coefficients, regardless of which isomer is prepared as the reactant.

Figures 11 and 12 compare our predictions of the allene and propyne dissociation rate coefficients, respectively, with the shock-tube data of Wu and Kern[45] and Hidaka et al.[46] Note that the rate coefficients are cast in bimolecular form. We should also note that, as one might expect from the potential energy surface, the theory indicates that completely negligible quantities of the C_3H_2 isomers are formed in the dissociation (the barriers for H_2 elimination are too high, and the corresponding transition states too tight). Consequently, the only significant products are $C_3H_3 + H$; the total rate coefficient for H_2 elimination is typically about 3 orders of magnitude (or more) smaller than that for C−H fission. In both experimental investigations, the dissociation rate coefficients were obtained indirectly by modeling the time history of the pyrolysis products. Much of the difference between theory and experiment is likely due to the indirectness of the experimental observations. However, our calculations were done with argon as a bath gas, rather than neon, which was used as a diluent by Wu and Kern (Hidaka used argon). If we had done our calculations with neon and kept the same $P(E,E')$ function, our agreement with Wu and

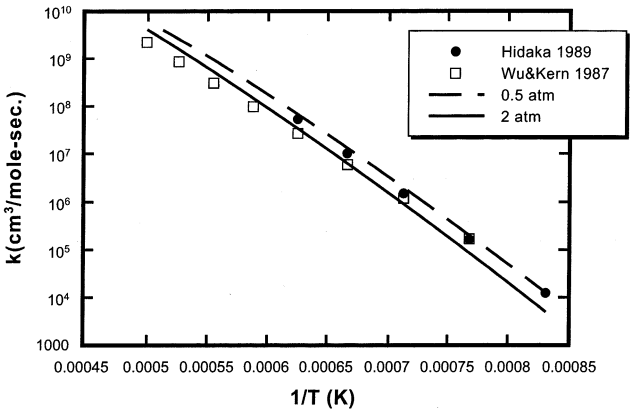

Figure 12. Comparison of the theory for the rate coefficient of $C_3H_4p + Ar \rightarrow C_3H_3 + H + Ar$ with the experiments of Hidaka et al.[46] and Wu and Kern.[45] The pressures used in the experiments are given in Figure 9. The symbols are points of the Arrhenius functions given in the experimental papers, not experimental data points.

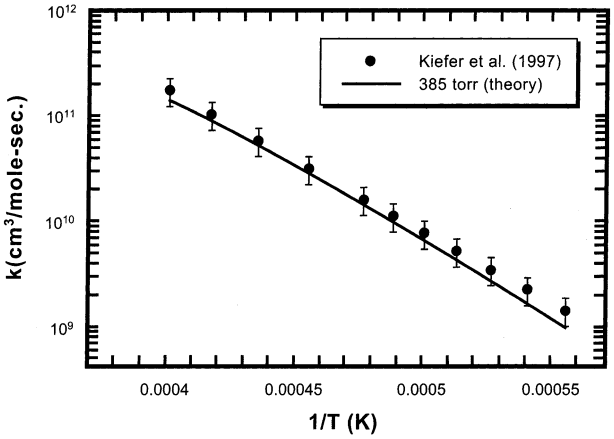

Figure 13. Comparison of the theory for the rate coefficient of $C_3H_4a + Kr \rightarrow C_3H_3 + H + Kr$ with the experiments of Kiefer et al.[40] The symbols are points through the center of Kiefer's data, and the error bars are indicative of the scatter. The pressures in the experiments were 70−700 Torr.

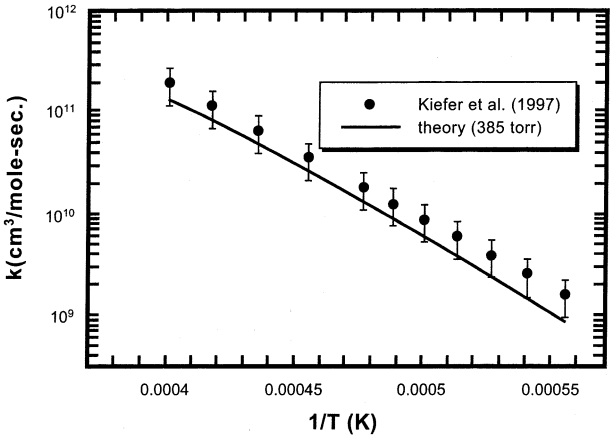

Figure 14. Comparison of the theory for the rate coefficient of $C_3H_4p + Kr \rightarrow C_3H_3 + H + Kr$ with the experiments of Kiefer et al.[40] The symbols are points through the center of Kiefer's data, and the error bars are indicative of the scatter. The pressures of the experiments were in the range 70−700 Torr.

Kern's experiments would be slightly worse because of the smaller collision rate for neon. It also seems unlikely that we could compensate satisfactorily for the difference between theory and experiment by making a realistic change in $\langle \Delta E_d \rangle$. It is noteworthy that Hidaka's experiments indicate that C_3H_4p dissociates faster than C_3H_4a by more than a factor of 2, whereas the theory indicates that allene dissociates faster, but only by 10−20%. Wu and Kern give the same rate-coefficient expression for the dissociation of both isomers.

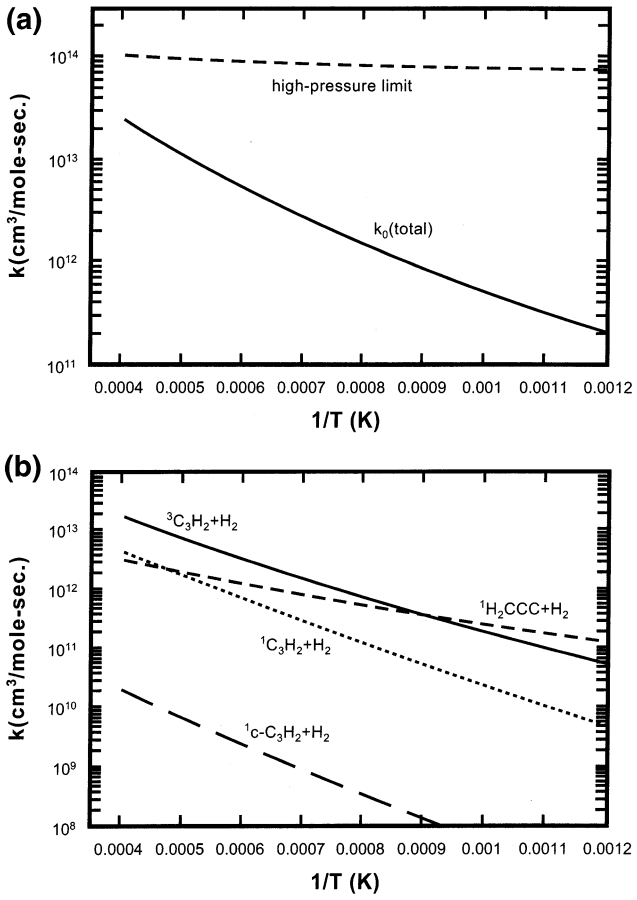

Figure 15. Rate coefficients for the bimolecular channels in the collisionless limit. Calculations were done with a two-dimensional ME; the one-dimensional calculations are virtually indistinguishable from the 2-d results.

Kiefer et al.[40] attempted to measure the dissociation rate coefficients of both C_3H_4p and C_3H_4a in a shock tube at 1800 K < T < 2500 K for pressures between 70 and 700 Torr using the laser-schlieren technique; krypton was the diluent. Although separating the rate coefficients of the two isomers is still problematic, their experiments have a better chance of doing so than most others. The contribution to the laser-schlieren signal from any chemical reaction is proportional to its rate times its endothermicity. Because it is nearly thermoneutral, the propyne $\rightleftarrows$ allene isomerization does not contribute directly to the signal. Kiefer et al. make their first measurement roughly 1 μs after passage of the shock with a time resolution considerably smaller than 1 μs. Our calculations indicate that it is only at the highest temperatures and pressures considered that the isomerization equilibrates in less than a microsecond; more commonly this equilibration takes a number of microseconds and as long as 10 μs for the lowest temperatures and pressures encountered. Consequently, we conclude that the competing isomerization is a problem, but perhaps not an insurmountable one.

In any event, we compare our theoretical predictions for the propyne and allene dissociation rate coefficients with the experimental results of Kiefer et al. in Figures 13 and 14. The agreement between theory and experiment is very good in that our calculations (using krypton as the bath gas) at p = 385 Torr (the median pressure of the experiments) fall within the scatter

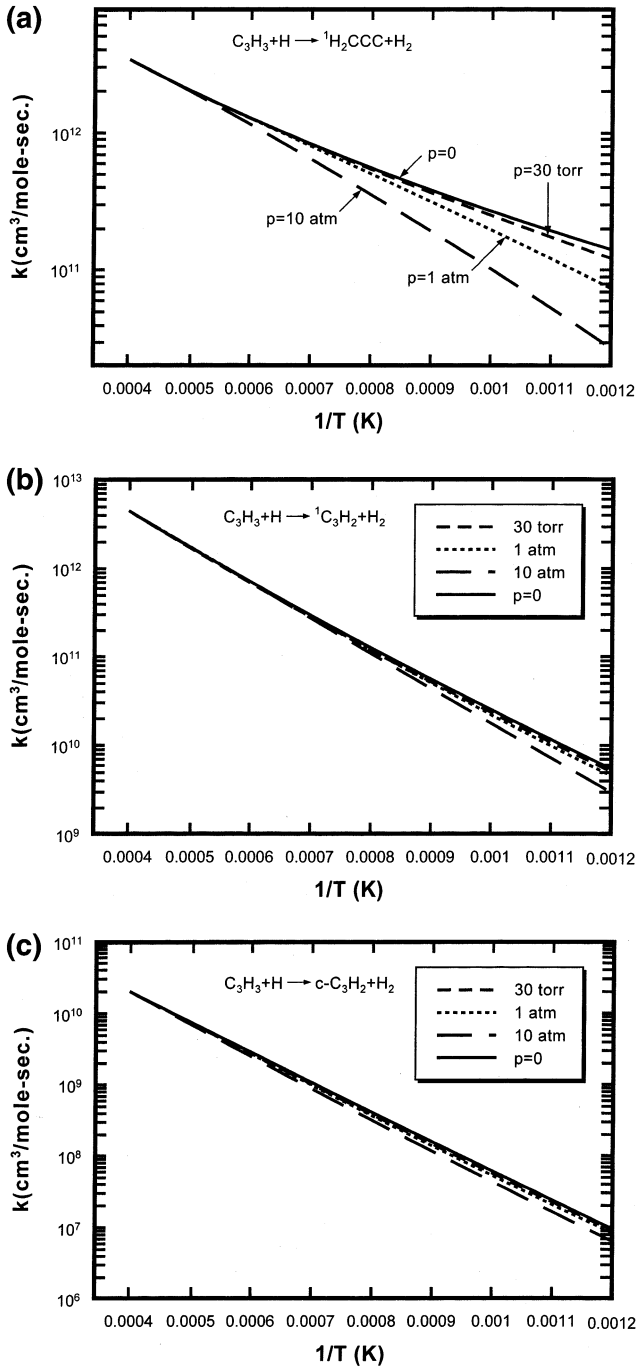

Figure 16. Pressure dependence of the bimolecular rate coefficients: (a) $C_3H_3 + H \rightarrow {}^1H_2CCC + H_2$ (b) $C_3H_3 + H \rightarrow {}^1C_3H_2 + H_2$ (c) $C_3H_3 + H \rightarrow c\text{-}C_3H_2 + H_2$.

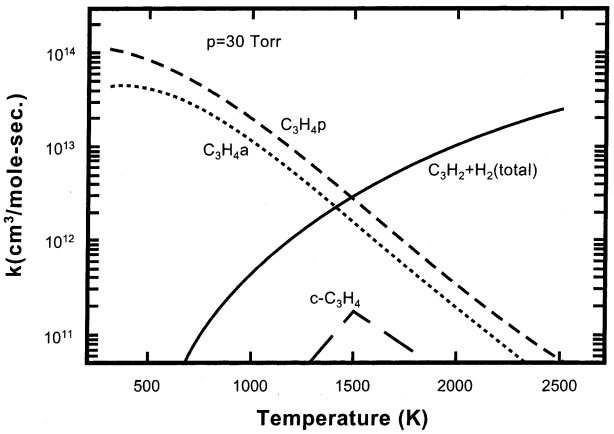

Figure 17. Rate coefficients for the reactions indicated at 30 Torr.

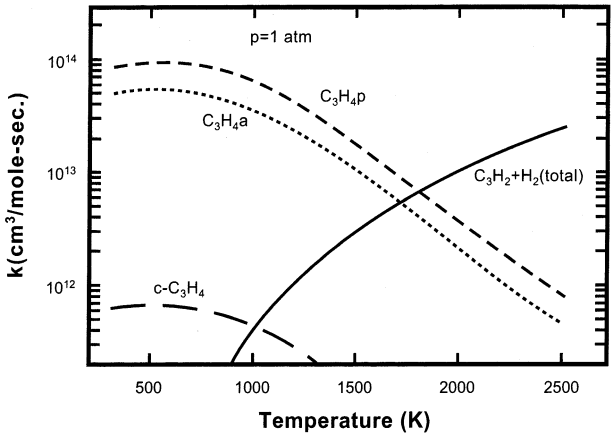

Figure 18. Rate coefficients for the reactions indicated at 1 atm.

of the data for both rate coefficients, although the agreement is somewhat better for allene. Our calculations indicate that allene dissociates about 10−20% faster than propyne, whereas the experiments show the reverse trend. Such small differences could be the fault of either the theory or the experiment. Unambiguous interpretation of the experiments is difficult for reasons discussed in the last paragraph, and a more accurate anharmonic state count conceivably could reverse the trend in the theory.

$C_3H_3 + H \rightarrow$ Products. From a combustion-chemistry point of view, perhaps the most important reaction on our C_3H_4 potential (i.e., excluding $^1CH_2 + C_2H_2$) is the reaction between propargyl and hydrogen atoms. The C_3H_4 complexes formed in such a reaction can be collisionally stabilized to form C_3H_4p, C_3H_4a, or c-C_3H_4, or they can go on to form one of the C_3H_2 isomers and H_2. There is also the direct abstraction to form triplet propargylene + H_2 on the triplet surface. Of course, we would like to know the rate coefficients for all of these steps to use in flame modeling.

Figure 15 displays our results for the bimolecular channels calculated using the two-dimensional, collisionless master equation described in section II; the one-dimensional ME results are virtually identical. The a frame of the figure compares the total collisionless rate coefficient for all of the bimolecular channels to the total capture rate coefficient (plus abstraction), i.e., the high-pressure limit. The b frame of the figure shows the speciation of the products in the collisionless limit. Up to a temperature of approximately 1100 K, the ^1H_2CCC (singlet propadienylidene) + H_2 channel is dominant (primarily through 1,1 elimination of H_2 from allene); for $T > 1100$ K, the direct abstraction to form $^3C_3H_2 + H_2$ takes over. Interestingly, ^{1}c-C_3H_2 is never an important product, even though it is the most stable thermodynamically of all of the C_3H_2 isomers.

Figure 16 shows the pressure dependence of the rate coefficients for formation of the singlet C_3H_2 isomers; of course, the direct abstraction has no pressure dependence. Argon was used as the bath gas in all of the ME calculations shown in Figure 16. Only the $^1H_2CCC + H_2$ channel shows substantial pressure dependence at combustion temperatures, and its dependence on p is quite large. Comparing Figures 15 and 16, one can see that the rate coefficient for $^1H_2CCC + H_2$ decreases so much with increasing pressure that $^3C_3H_2 + H_2$ becomes the dominant bimolecular channel, over the entire temperature range shown, at a pressure somewhere between 1 and 10 atm.

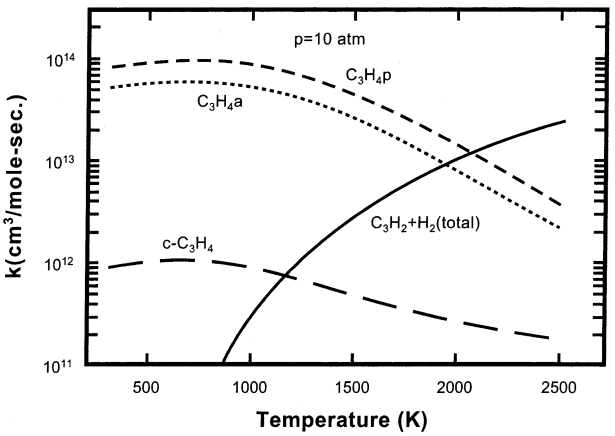

Figure 19. Rate coefficients for the reactions indicated at 10 atm.

TABLE 4: Rate Coefficients for the Indicated Reactions in Modified Arrhenius Form $k = AT^n \exp(-E_0/RT)$[a]

reaction	log *A*	*n*	E_0	temperature range (K)
		$p = 0$		
$C_3H_3 + H \rightarrow {}^1H_2CCC + H_2$	9.14	1.12	4811	800−2500
$C_3H_3 + H \rightarrow {}^1C_3H_2 + H_2$	8.42	1.57	12 571	800−2500
$C_3H_3 + H \rightarrow$ c-$C_3H_2 + H_2$	3.96	2.23	13 400	800−2500
$C_3H_3 + H \rightarrow {}^3C_3H_2 + H_2$	5.33	2.52	7453	800−2500
		$p = 30$ Torr		
$C_3H_3 + H \rightarrow {}^1H_2CCC + H_2$	9.43	1.05	5371	800−2500
$C_3H_3 + H \rightarrow {}^1C_3H_2 + H_2$	9.47	1.28	13 474	800−2500
$C_3H_3 + H \rightarrow$ c-$C_3H_2 + H_2$	7.03	1.37	15 557	800−2500
$C_3H_4a \rightarrow C_3H_4p$	53.78	−12.18	84 276	800−2500
c-$C_3H_4 \rightarrow C_3H_4p$	50.40	−11.82	50 914	800−2500
c-$C_3H_4 \rightarrow C_3H_4a$	43.99	−9.97	56 007	800−2500
$C_3H_3 + H \rightarrow C_3H_4p$	36.56	−7.36	6039	300−2000
$C_3H_3 + H \rightarrow C_3H_4a$	36.53	−7.41	6337	300−2000
$C_3H_3 + H \rightarrow$ c-C_3H_4	112.95	−28.26	83 611	1000−2000
		$p = 1$ atm		
$C_3H_3 + H \rightarrow {}^1H_2CCC + H_2$	13.46	−0.03	9448	800−2500
$C_3H_3 + H \rightarrow {}^1C_3H_2 + H_2$	10.04	1.13	13 929	800−2500
$C_3H_3 + H \rightarrow$ c-$C_3H_2 + H_2$	7.13	1.34	15 560	800−2500
$C_3H_4a \rightarrow C_3H_4p$	39.89	−7.80	78 446	800−2500
c-$C_3H_4 \rightarrow C_3H_4p$	37.09	−7.51	45 551	800−2000
c-$C_3H_4 \rightarrow C_3H_4a$	26.40	−4.56	43 922	800−2000
$C_3H_3 + H \rightarrow C_3H_4p$	29.90	−5.06	4861	300−2000
$C_3H_3 + H \rightarrow C_3H_4a$	29.50	−5.00	4711	300−2000
$C_3H_3 + H \rightarrow$ c-C_3H_4	21.03	−2.95	2687	300−2000
		$p = 10$ atm		
$C_3H_3 + H \rightarrow {}^1H_2CCC + H_2$	18.00	−1.23	15 111	800−2500
$C_3H_3 + H \rightarrow {}^1C_3H_2 + H_2$	13.52	0.195	17 579	800−2500
$C_3H_3 + H \rightarrow$ c-$C_3H_2 + H_2$	9.86	0.606	18 356	800−2500
$C_3H_4a \rightarrow C_3H_4p$	48.68	−10.00	88 685	800−2500
c-$C_3H_4 \rightarrow C_3H_4p$	37.22	−7.24	48 013	800−2000
c-$C_3H_4 \rightarrow C_3H_4a$	35.70	−6.87	51 298	800−2000
$C_3H_3 + H \rightarrow C_3H_4p$	24.03	−3.15	3261	300−2000
$C_3H_3 + H \rightarrow C_3H_4a$	23.94	−3.20	3255	300−2000
$C_3H_3 + H \rightarrow$ c-C_3H_4	18.51	−2.05	2053	300−2000

[a] Units are cm^3, moles, seconds, kelvins, calories/mole. Molecularity is as indicated.

Figures 17−19 display the rate coefficients for the three stabilization products and the total bimolecular rate coefficient as a function of temperature for three pressures: 30 Torr (typical of low-pressure flame experiments), 1 atm, and 10 atm. Again, argon was used as the bath gas in the ME calculations. Under all conditions that we investigated, propyne is the dominant stabilization product; the rate coefficient for allene formation is slightly less than a factor of 2 smaller than that for propyne, and that for c-C_3H_4 production is generally not important. Figure 17 shows that, in a 30 Torr flame, the bimolecular channels begin to dominate the reaction at a temperature of about 1600 or 1700 K, whereas Figure 19 shows that one must raise the temperature to well over 2000 K at 10 atm for the bimolecular channels to dominate.

There are relatively few experimental data with which to compare our predictions for the C_3H_3 + H rate coefficients. Harding and Klippenstein have already compared the theoretical results for the high-pressure limit with experiment at low temperature, so we do not repeat that comparison here. Rate coefficients for the bimolecular products used in combustion modeling[3,51−53] are larger than those given here. It remains to be seen what effect the smaller rate coefficients might have on any of those models. Of course, it is possible that our barrier heights are too large (an error of 3 kcal/mol would not be out of the question) and that the true rate coefficients are somewhat larger than our predictions.

Rate Coefficients for Chemical Kinetic Modeling. Table 4 gives rate coefficients in modified Arrhenius form for the elementary reactions discussed in this article. These expressions are intended for use in combustion modeling and are given for a variety of (fixed) pressures. The temperature range over which the fits were made is indicated in the table. Generally, the modified Arrhenius functions are good to at least ±20% in the temperature range shown. In some cases, they become bad very quickly outside that range. This is the case most notably for the stabilization reactions for $T > 2000$ K.

IV. Concluding Remarks

In the present article, we have used a combination of electronic-structure theory, RRKM theory (for microcanonical rate coefficients), and master-equation methodology to predict the temperature- and pressure-dependent thermal rate coefficients for a variety of elementary reactions that occur on the C_3H_4 potential. We have compared our predictions with the experimental data available in all cases. The results clearly demonstrate the utility of the master-equation methodology in predicting thermal rate coefficients for chemical reactions that take place over multiple, interconnected potential wells. Table 4 gives modified Arrhenius expressions for a number of elementary reactions for use in chemical kinetics modeling.

Acknowledgment. This work was supported by the United States Department of Energy, Office of Basic Energy Sciences, Division of Chemical Sciences, Geosciences, and Biosciences.

References and Notes

(1) Miller, J. A. *Proc. Combust. Inst.* **1996**, *20*, 461−480.
(2) Miller, J. A. *Faraday Discuss.* **2001**, *119*, 461−475.
(3) Miller, J. A.; Melius, C. F. *Combust. Flame* **1992**, *91*, 21.
(4) Hahn, D. K.; Klippenstein, S. J.; Miller, J. A. *Faraday Discuss.* **2001**, *119*, 79−100.
(5) Melius, C. F.; Miller, J. A.; Evleth, E. M. *Proc. Combust. Inst.* **1992**, *24*, 621−628.
(6) Blitz, M. A.; Beasley, M. S.; Pilling, M. J.; Robertson, S. A. *Phys. Chem. Chem. Phys.* **2000**, *2*, 905−912.
(7) Frankcombe, T. J.; Smith, S. C., *Faraday Discuss.* **2001**, *119*, 159.
(8) Harding, L. B.; Klippenstein, S. J. *Proc. Combust. Inst.* **2000**, *28*, 1503−1509.
(9) Miller, J. A.; Klippenstein, S. J.; Robertson, S. H. *J. Phys. Chem. A* **2000**, *104*, 7525−7536; *J. Phys. Chem. A* **2000**, *104*, 9806 (correction).
(10) Miller, J. A.; Klippenstein, S. J., Robertson, S. H. *Proc. Combust. Inst.* **2000**, *28*, 1479.
(11) Miller, J. A.; Klippenstein, S. J. *Int. J. Chem. Kinet.* **2001**, *33*, 654−668.
(12) Miller, J. A.; Klippenstein, S. J. *J. Phys. Chem. A* **2001**, *105*, 7254−7266.
(13) Miller, J. A.; Klippenstein, S. J.; Raffy, C. *J. Phys. Chem. A* **2002**, *106*, 4904−4913.

(14) Miller, J. A.; Parrish, C.; Brown, N. J. *J. Phys. Chem.* **1986**, *90*, 3339.
(15) Klippenstein, S. J.; Miller, J. A, *J. Phys. Chem. A* **2002**, 106, 9267−9277.
(16) Miller, J. A.; Klippenstein, S. J. *J. Phys. Chem. A* **2000**, *104*, 2061−2069.
(17) Becke, A. D. *J. Chem. Phys.* **1993**, *98***,** 5648.
(18) Hehre, W. J.; Radom, L.; Pople. J. A.; Schleyer, P. v. R. *Ab Initio Molecular Orbital Theory*; Wiley: New York, 1987.
(19) Curtiss, L. A.; Raghavachari, K.; Redfern, P. C.; Rassolov, V.; Pople, J. A. *J. Chem. Phys.* **1998**, *109*, 7764.
(20) Martin, J. M. L. *Chem. Phys. Lett.* **1996**, *259*, 669.
(21) Dunning, T. H. *J. Chem. Phys*. **1989**, *90*, 1007.
(22) Frisch, M. J.; Trucks, G. W.; Schlegel, H. B.; Scuseria, G. E.; Robb, M. A.; Cheeseman, J. R.; Zakrzewski, V. G.; Montgomery, J. A., Jr.; Stratmann, R. E.; Burant, J. C.; Dapprich, S.; Millam, J. M.; Daniels, A. D.; Kudin, K. N.; Strain, M. C.; Farkas, O.; Tomasi, J.; Barone, V.; Cossi, M.; Cammi, R.; Mennucci, B.; Pomelli, C.; Adamo, C.; Clifford, S.; Ochterski, J.; Petersson, G. A.; Ayala, P. Y.; Cui, Q.; Morokuma, K.; Malick, D. K.; Rabuck, A. D.; Raghavachari, K.; Foresman, J. B.; Cioslowski, J.; Ortiz, J. V.; Stefanov, B. B.; Liu, G.; Liashenko, A.; Piskorz, P.; Komaromi, I.; Gomperts, R.; Martin, R. L.; Fox, D. J.; Keith, T.; Al-Laham, M. A.; Peng, C. Y.; Nanayakkara, A.; Gonzalez, C.; Challacombe, M.; Gill, P. M. W.; Johnson, B.; Chen, W.; Wong, M. W.; Andres, J. L.; Gonzalez, C.; Head-Gordon, M.; Replogle, E. S.; Pople, J. A. *Gaussian 98*; Gaussian, Inc.: Pittsburgh, PA, 1998.
(23) Widom, B. *Science* **1965**, *148*, 1555−1560.
(24) Widom, B. *J. Chem. Phys*. **1971**, *55*, 44−52.
(25) Widom, B. *J. Chem. Phys*. **1974**, *61*, 672−680.
(26) Bartis, J. T.; Widom, B. *J. Chem. Phys.* **1974**, *60*, 3474−3482.
(27) Klippenstein, S. J.; Wagner, A. F.; Dunbar, R. C.; Wardlaw, D. M.; Robertson, S. H.; Miller, J. A. VARIFLEX version 1.12m, 2002.
(28) Pople, J. A.; Head-Gordon, M.; Raghavachari, K. *J. Chem. Phys*. **1987**, *87*, 5968.
(29) Honjou, N.; Pacansky, J.; Yoshimine, M. *J. Am. Chem. Soc*. **1984**, *106*, 5361.
(30) Honjou, N.; Pacansky, J.; Yoshimine, M. *J. Am. Chem. Soc*. **1985**, *107*, 5332.
(31) Kakumoto, T.; Ushirogouchi, T.; Saito, K.; Imamura, A. *J. Phys. Chem*. **1987**, *91*, 183.
(32) Karni, M.; Oref, I.; Barzilai-Gilboa, S.; Lifshitz, A. *J. Phys. Chem*. **1988**, *92*, 6924−6929.
(33) Yoshimine, M.; Pacansky, J.; Honjou, N. *J. Am. Chem. Soc*. **1989**, *111*, 2785−2798.
(34) Yoshimine, M.; Pacansky, J.; Honjou, N. *J. Am. Chem. Soc*. **1989**, *111*, 4198−4209.
(35) Bauschlicher, C. W.; Langhoff, S. R. *Chem. Phys. Lett*. **1992**, *193*, 380.
(36) Kiefer, J. H.; Kumuran, S. S.; Mudipalli, P. S. *Chem. Phys. Lett*. **1994**, *224*, 51−55.
(37) Walch, S. P. *J. Chem. Phys*. **1995**, *103*, 7064−7071.
(38) Bettinger, H. F.; Schreiner, P. R.; Schleyer, P. v. R.; Schaefer, H. F. *J. Phys. Chem.* **1996**, *100*, 16147−16154.
(39) Kakkar, R.; Padhi, B. S. *Int. J. Quantum Chem*. **1996**, *58*, 389.
(40) Kiefer, J. H.; Mudipalli, P. S.; Sidhu, S. S.; Kern, R. D.; Jursic, B. S.; Xie, K.; Chen, H. *J. Phys. Chem. A* **1997**, *101*, 4057−4071.
(41) Jackson, W. M.; Mebel, A. M.; Lin, S. H.; Lee, Y. T. *J. Phys. Chem. A* **1997**, *101*, 6638.
(42) Mebel, A. M.; Jackson, W. M.; Chang, A. H. H.; Lin, S. H. *J. Am. Chem. Soc.* **1998**, *120*, 5751−5763.
(43) Davis, S. G.; Law, C. K.; Wang, H. *J. Phys. Chem. A* **1999**, *103*, 5889−5899.
(44) Bailey, I. M.; Walsh, R. J. *J. Chem Soc., Faraday Trans. 1* **1978**, *74*, 1146.
(45) Wu, C. H.; Kern, R. D. *J. Phys. Chem.* **1987**, *91*, 6291.
(46) Hidaka, Y.; Nakamura, T.; Miyauchi, A.; Shiraishi, T.; Kawano, H. *Int. J. Chem. Kinet*. **1989**, *21*, 643.
(47) Levush, S. S.; Abadzhev, S. S.; Shevchuk, V. U. *Neftechimia* **1969**, *9*, 215.
(48) Lifshitz, A.; Frenklach, M.; Burcat, A. *J. Phys. Chem*. **1975**, *79*, 1148.
(49) Hidaka, Y.; Chimori, T.; Suga, M. *Chem. Phys. Lett.* **1985**, *119*, 435.
(50) Bradley, J. N.; West, K. O. *J. Chem Soc., Faraday Trans. 1* **1975**, *71*, 967.
(51) Miller, J. A.; Volponi, J. V.; Pauwels, J.-F. *Combust. Flame* **1996**, *105*, 451.
(52) Pauwels, J.-F.; Volponi, J. V.; Miller, J. A. *Combust. Sci. Technol*. **1995**, *110*−*111*, 249.
(53) Pope, C. J.; Miller, J. A. *Proc. Combust. Inst.* **2000**, *28*, 1519.